ISSN: 1410-8917
Jurnal Kimia Sains & Aplikasi
e-ISSN: 2597-9914

Jurnal Kimia Sains dan Aplikasi 28 (7) (2025): 396-404

Jurnal Kimia Sains dan Aplikasi
Journal of Scientific and Applied Chemistry

Journal homepage: http://ejournal.undip.ac.id/index.php/ksa

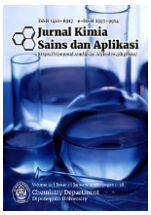

Synthesis and Characterization of rGO Using a Combination Hummers Method and Hydrothermal Reduction

Maichel Letare Pardede [1], Nicholas Jonathan [1], Robin Irawan [1], Agung Nugroho [2], Ratna Frida Susanti [1,*]

[1] Center for Advanced Product Development and Materials Studies, Department of Chemical Engineering, Faculty of Engineering Technology, Parahyangan Catholic University, Bandung, Indonesia
[2] Department of Chemical Engineering, Faculty of Industrial Technology, Universitas Pertamina, Jakarta Selatan, DKI Jakarta, Indonesia

* Corresponding author: santi@unpar.ac.id

https://doi.org/10.14710/jksa.28.7.396-404

Article Info

Article history:

Received: 21st May 2025
Revised: 17th August 2025
Accepted: 20th August 2025
Online: 10th September 2025

Keywords:
reduced graphene oxide; XRD; graphite oxide; Hummer; supercapacitor

Abstract

Reduced graphene oxide (rGO) was successfully synthesized through a combination of two synthesis methods. The Hummers method was employed to synthesize graphite oxide (GrO), followed by a hydrothermal reduction technique to obtain a more ordered rGO structure. X-ray diffraction (XRD) analysis confirmed the transformation of GrO to rGO, as indicated by an interlayer spacing of 0.35–0.40 nm. This value reflects the crystalline characteristics and multilayer nature of the structure. The calculated crystallite size yielded L_a = 5.825 nm and L_c = 0.967 nm, suggesting a relatively high degree of crystallinity. Raman spectroscopy revealed an increase in structural disorder after the reduction process, as shown by an I_{D1}/I_G ratio of 1.771, which indicates the formation of structural defects due to the removal of oxygen-containing groups. Meanwhile, the I_G/I_{D3} ratio of 1.039 confirms that the carbon atoms in rGO are arranged in a hexagonal graphite lattice. Additionally, the I_{2D}/I_G ratio of 0.321 indicates the presence of a multilayer structure. Scanning electron microscopy coupled with energy-dispersive X-ray spectroscopy (SEM-EDX) showed that the rGO consists of graphene layers exhibiting folding and wrinkling, likely caused by thermal fluctuations during reduction at 180°C. The success of the reduction process was further supported by the increase in the C/O ratio from 2.42 in GrO to 5.39 in rGO. Electrochemical characterization by cyclic voltammetry (CV) demonstrated that rGO exhibits pseudocapacitive behavior, achieving a specific capacitance of 408.661 F/g at a scan rate of 5 mV/s. Overall, the combined synthesis approach employed in this study successfully produced rGO with favorable morphology and promising electrochemical properties, highlighting its potential for energy storage applications such as supercapacitors.

1. Introduction

Graphene is among the most extensively studied carbon-based materials, attracting considerable research interest because of its remarkable electrical properties and large surface area [1]. It is a two-dimensional (2D) crystal composed of a single layer of sp^2-hybridized carbon atoms arranged in a hexagonal lattice. This unique structure of graphene confers excellent mechanical and electrical properties due to its planar σ and π bonding network. Additionally, graphene is the thinnest and most flexible known crystal, exhibiting outstanding thermal conductivity and high electron mobility [2, 3, 4]. Despite these superior properties, large-scale production of high-quality graphene remains a major challenge due to the complexity of synthesis methods and high production costs [1]. In contrast, graphene oxide (GO) can be produced in large quantities at relatively low cost. However, its electrical conductivity is much lower than that of pristine graphene [5].

Reduced graphene oxide (rGO) has thus emerged as a promising alternative, offering properties comparable to those of graphene. The reduction of GO is currently

considered the most practical and scalable approach for producing graphene-like materials. This process can be achieved through chemical, thermal, or electrochemical methods, each yielding products with varying similarity to pure graphene in terms of electrical, thermal, and mechanical properties, as well as surface morphology [1, 3, 6, 7, 8, 9, 10].

rGO continues to be developed for various applications, including supercapacitors, sensors, batteries, and membranes [1, 11, 12, 13]. Among these, the use of rGO as a supercapacitor electrode material continues to be an active area of research. Supercapacitors have become a key component in modern energy storage technologies due to their ability to store and release energy rapidly, as well as their long cycle life. Unlike conventional batteries, supercapacitors store energy electrostatically without significant chemical reactions, which enables more stable performance and higher efficiency [8, 9]. In particular, rGO has been identified as a promising supercapacitor electrode material owing to its high electrical conductivity, large specific surface area, and chemical tunability [14]. The quality of rGO is strongly dependent on the quality of graphite oxide (GrO) or graphene oxide (GO), which serve as intermediate products derived from graphite as the primary raw material.

In this study, graphite was used as the precursor for the synthesis of GrO, which was subsequently sonicated to obtain GO and then reduced to rGO. The synthesis combined a modified Hummers method with the approach reported by Al-Gaashani *et al.* [15] for GO preparation [16]. During the GrO synthesis, a graphite-to-$KMnO_4$ ratio of 1:9 was applied to achieve an optimal oxidation reaction [17]. Only H_2SO_4 and $KMnO_4$ were used as oxidizing agents, avoiding $NaNO_3$ in order to minimize the release of toxic gases (NO_2 and N_2O_4) and to prevent residual Na^+ and NO_3^- ions, which are difficult to remove during the washing of acidic GO suspensions [10, 18]. This strategy is expected to enhance the quality of GrO while making the synthesis process more environmentally friendly.

Beyond synthesis, this study also evaluates the electrochemical performance of the obtained rGO for supercapacitor applications. The results are expected to provide meaningful contributions to the development of more efficient and sustainable GO synthesis methods, particularly for use as supercapacitor electrodes.

To evaluate the quality of the synthesized rGO, comprehensive characterization was performed. X-ray diffraction (XRD) was used to determine the crystallite size along the in-plane (a-axis, L_a) and out-of-plane (c- axis, L_c) directions, the degree of crystallinity, and the number of layers (N). Raman spectroscopy was employed to assess the defect density and degree of graphitization, while scanning electron microscopy coupled with energy-dispersive X-ray spectroscopy (SEM-EDX) provided information on morphology and the efficiency of the reduction process. The electrochemical performance of rGO as a supercapacitor electrode was assessed using a three-electrode system [19]. This study serves as a preliminary step in evaluating the potential of the synthesized rGO for supercapacitor applications.

2. Experimental

2.1. Materials

Graphite powder (<20 µm, Merck, 99%) was used as the raw material for rGO synthesis. All other chemicals were of analytical grade, including sulfuric acid (H_2SO_4, Merck, 98%), potassium permanganate ($KMnO_4$, Merck, 99%), hydrochloric acid (HCl, Mekar Pancaraya, 10%), hydrogen peroxide (H_2O_2, Brataco, 30%), distilled water, and reverse osmosis (RO) water.

2.2. Equipment

The equipment used for rGO synthesis included a Teflon-lined autoclave reactor for the reduction of GO to rGO, an oven for heating during the hydrothermal reduction process, and a hotplate for the GrO synthesis process. A magnetic stirrer was employed for mixing, while an ice-water bath was used to control the exothermic reaction. An ultrasonic bath was utilized for GrO exfoliation, and a Buchner funnel coupled with a vacuum pump was applied for washing rGO. Additional laboratory equipment included beakers, stirring rods, measuring cylinders, evaporation dishes, an analytical balance, and a desiccator.

2.3. Synthesis of GrO

GrO was synthesized using a modified Hummers method [15, 18]. Graphite powder (1 g) was dispersed in 100 mL of concentrated H_2SO_4 (98%) while maintaining the temperature at 5°C using an ice-water bath under continuous stirring. $KMnO_4$ (9 g) was then added slowly to control the highly exothermic reaction, with the mixture kept in the ice bath to maintain the temperature at approximately 5°C. The suspension was subsequently stirred for 1 h at 75°C.

Afterward, 100 mL of distilled water was slowly added dropwise using a burette, and stirring was continued for 1 h while maintaining the temperature at 75°C. To terminate the oxidation reaction, 15 mL of H_2O_2 was followed by 120 mL of distilled water. The resulting yellowish suspension was allowed to precipitate overnight to separate the GrO layers formed during oxidation.

The precipitate was washed with 15 mL of 10% HCl to remove residual metal ions (e.g., Mn^{2+}) and then left to settle for 12 h [14]. The resulting blackish precipitate was separated from the acid solution and washed repeatedly by centrifugation at 6000 rpm until a neutral pH was reached. The gel-like product obtained after washing was dried in a vacuum oven at 60°C for 24 h to yield solid GrO. The overall synthesis process is illustrated in Figure 1.

2.4. Synthesis of Reduced Graphene Oxide (rGO)

rGO was synthesized by dispersing GrO powder in reverse osmosis (RO) water at a concentration of 5 mg/mL (15 mL total volume). The suspension was sonicated for 2 h to exfoliate the GrO sheets into graphene oxide (GO) and ensure uniform dispersion, thereby facilitating an effective reduction process.

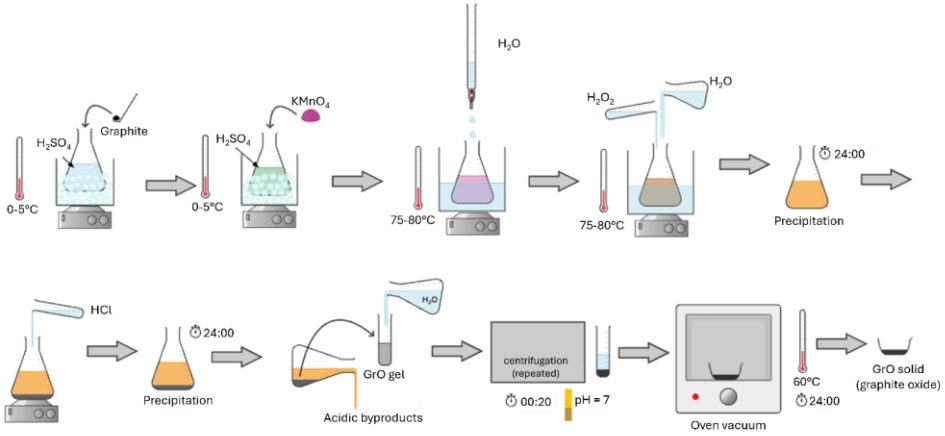

Figure 1. GrO synthesis process

Following sonication, the suspension was transferred to a 20 mL Teflon-lined autoclave, sealed, and heated in an oven at 180°C for 24 h [20]. This hydrothermal treatment initiated the reduction of GO to rGO under high-temperature and high-pressure conditions. The resulting product was washed repeatedly with RO water using a Buchner funnel to remove residual reactive species and by-products such as Cl^-, SO_4^{2-}, and Mn^{2+} [21]. Finally, the washed product was dried in a vacuum oven at 60°C for 12 h to remove residual moisture, ensuring stable physical and chemical properties of the rGO for subsequent characterization and applications.

2.5. Characterization of rGO

The characterization of rGO included analyses of morphology, elemental composition, surface functional groups, crystal structure, phase, crystallite size, and atomic ordering. Morphology and elemental composition were examined using scanning electron microscopy coupled with energy-dispersive X-ray spectroscopy (SEM-EDX) with a JSM-6510 Series microscope (JEOL, Japan). X-ray diffraction (XRD) measurements were performed with a Rigaku Miniflex 600 diffractometer (LANScientific Co., Ltd., China) to evaluate the crystal structure of the rGO samples. Raman spectroscopy (iHR 320, Horiba, Japan) was employed to determine the I_D/I_G intensity ratio, which reflects the degree of structural defects and the efficiency of GO reduction to rGO. The interlayer spacing (d) was calculated from the XRD patterns using Bragg's equation (Equation 1) [22, 23].

$$2d\ sin\theta = n\lambda \quad (1)$$

Where, n = 1

Meanwhile, the crystallite sizes, L_c and L_a, were calculated using the Scherrer equation (2) [23].

$$L = \frac{K\lambda}{\beta cos\theta} \quad (2)$$

Where, L is the average size of the crystallite domain, L_a is the crystallite size along the a-axis (in-plane direction), L_c is the crystallite size along the c-axis (out-of-plane direction), K is the shape factor (0.9), λ is the X- ray wavelength (0.15406 nm), and β is the full width at half maximum (FWHM) in radians. The L_c parameter was determined from the [002] peak, while L_a was determined from the [101] peak [23].

The number of layers (N) of rGO was calculated using Equation 3 [23].

$$N = \frac{L_c}{d} \quad (3)$$

2.6. Electrochemical Analysis

The electrochemical performance of the synthesized rGO was evaluated to determine its feasibility as a supercapacitor electrode. Cyclic voltammetry (CV) was employed to investigate the redox behavior and electrochemical kinetics of the material. Measurements were conducted using a three-electrode system with a Metrohm Autolab electrochemical workstation, where platinum served as the counter electrode, and a saturated calomel electrode was used as the reference electrode.

The working electrode was prepared by coating a glassy carbon electrode (diameter 0.3 cm, area 0.07065 cm^2) with rGO ink. The ink was prepared following the method of Le *et al.* [12] and Nugroho *et al.* [20], by dispersing 2 mg of rGO in 1 mL of isopropanol and air-drying for 10 min. Then, 3 µL Nafion solution was added as a binder and dried for another 10 min. Electrochemical measurements were performed in a 6 M KOH electrolyte. CV was recorded within a potential window of -0.5 to 0.5 V at scan rates of 5, 10, 20, 50, and 100 mV/s [20].

3. Results and Discussion

Standard characterization of sp^2 carbon materials was performed on rGO to evaluate its suitability as a supercapacitor electrode. These analyses included Raman spectroscopy, XRD, and SEM to examine the structural properties of rGO. XRD was first utilized to determine the basic crystalline pattern of rGO and to assess the success of the synthesis process.

XRD analysis was also performed on the intermediate product, GrO, to confirm the effectiveness of the hydrothermal reduction process, as indicated by the shift of the [002] diffraction peak. A comparison of the XRD patterns for GrO and rGO is presented in Figure 2a. The [002] peak of GrO appeared at 10.44°, corresponding to an interlayer spacing of 0.845 nm, which shifted following reduction. In rGO, a peak was observed at 25.26°, characteristic of reduced graphene oxide (Figure 2a) [22], and this peak was used to calculate the interlayer spacing (d-spacing).

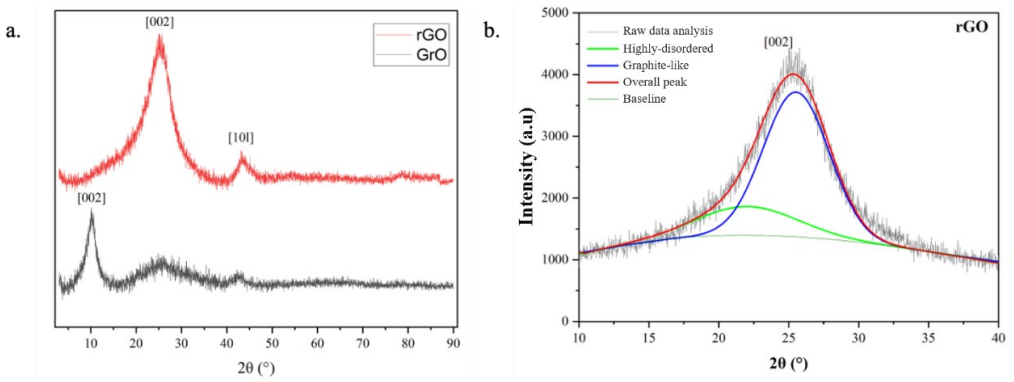

Figure 2. (a) XRD patterns of GrO and reduced graphene oxide (rGO), and (b) deconvolution of the [002] peak for rGO

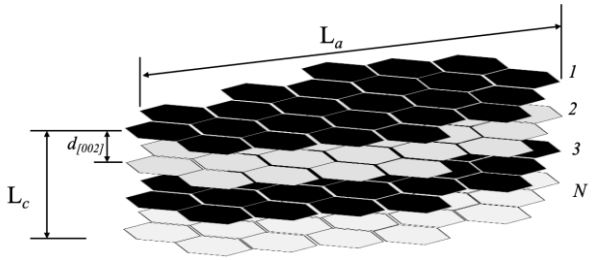

Figure 3. Schematic representation of rGO particles

XRD analysis also revealed the structural parameters of the microcrystallites. The lateral crystallite size (L_a) represents the average size of crystallites in the basal plane (sp^2), while the crystallite thickness (L_c) reflects the number of stacked graphite layers within a domain, indicating the degree of layer stacking. These structural parameters are illustrated in Figure 3.

Based on the d-spacing, carbon materials can be classified into three main types. Carbon phases with a d- spacing greater than 0.40 nm typically consist of highly disordered microcrystallites. The second category, with d-spacing between 0.36 and 0.40 nm, corresponds to pseudo-graphitic carbon, which is amorphous carbon exhibiting a relatively ordered microcrystalline structure. The third category comprises graphite-like carbon, characterized by d-spacing values below 0.36 nm [24].

In Figure 2b, the [002] peak was deconvoluted using Gaussian fitting in Origin Pro software to distinguish the graphite-like and highly disordered regions [24]. The 2θ and full width at half maximum (FWHM) values were obtained for each component peak. These values were then used to calculate the d-spacing using Bragg's equation (Equation 1). The resulting structural parameters are summarized in Table 1.

The main XRD peak of rGO appears at 2θ = 25.26°, indicating an improvement in the π-conjugated structure of graphene. The broad [002] peak suggests that the [002] crystal planes in rGO are randomly oriented, in contrast to highly crystalline graphite, which exhibits a sharp and intense [002] peak [25]. This observation is consistent with the study by Stobinski *et al.* [22] in which commercial rGO (Acros Organics, USA, 325 mesh) displayed a d- spacing (d_{002}) of 0.4 nm. Adequate d-spacing in rGO facilitates ion diffusion and enhances the material's energy storage capacity [26]. A comparison of the structural parameters of rGO is presented in Table 2.

Table 1. Structural parameters of rGO

Parameter	Peak deconvolution	
	Graphite-like	Highly disordered
Area	76.92%	23.08%
d[1]	0.349 nm	0.403 nm
N[2]	4.212	2.395
L_a[3]	5.825 nm	
L_c[4]	1.266 nm	

[1]Distance between layers
[2]the number of crystal layers that form a crystalline structure
[3]Crystallite size along the a-axis (in-plane direction),
[4]Crystallite size along the c-axis (out-of-plane direction)

Table 2. Comparison of structural parameters of rGO in this study and those reported by Stobinski *et al.* [22]

rGO parameter	This study	Stobinski *et al.* [22]
2θ (°) [002] peak	25.26	23.76
d_{002} (nm)	0.35 – 0.4	0.4
N	2-4	2-3

The number of layers (N) calculated using the Bragg equation was 2.395 for the highly disordered regions and 4.212 for the graphite-like regions, indicating that the rGO synthesized in this study is multilayered. The structural parameters of the synthesized rGO were comparable to those of commercial rGO reported by Stobinski *et al.* [22].

Figure 2b provides an indication of the crystallinity of rGO. The areas under the highly disordered and graphite-like peaks, obtained from deconvolution [24], were used to estimate the relative amorphous and crystalline fractions. The crystalline fraction was 76.92%, while the amorphous fraction was 23.08%, demonstrating that the rGO produced tends toward crystallinity. Additionally, a lower-intensity peak at 2θ = 43.32°, corresponding to the [101] orientation, was observed, which is associated with the turbostratic band and reflects structural irregularities in rGO. The prominent [002] peak confirms the success of the reduction process and the similarity of the synthesized rGO to commercial rGO, which typically contains 2–4 graphene layers [22].

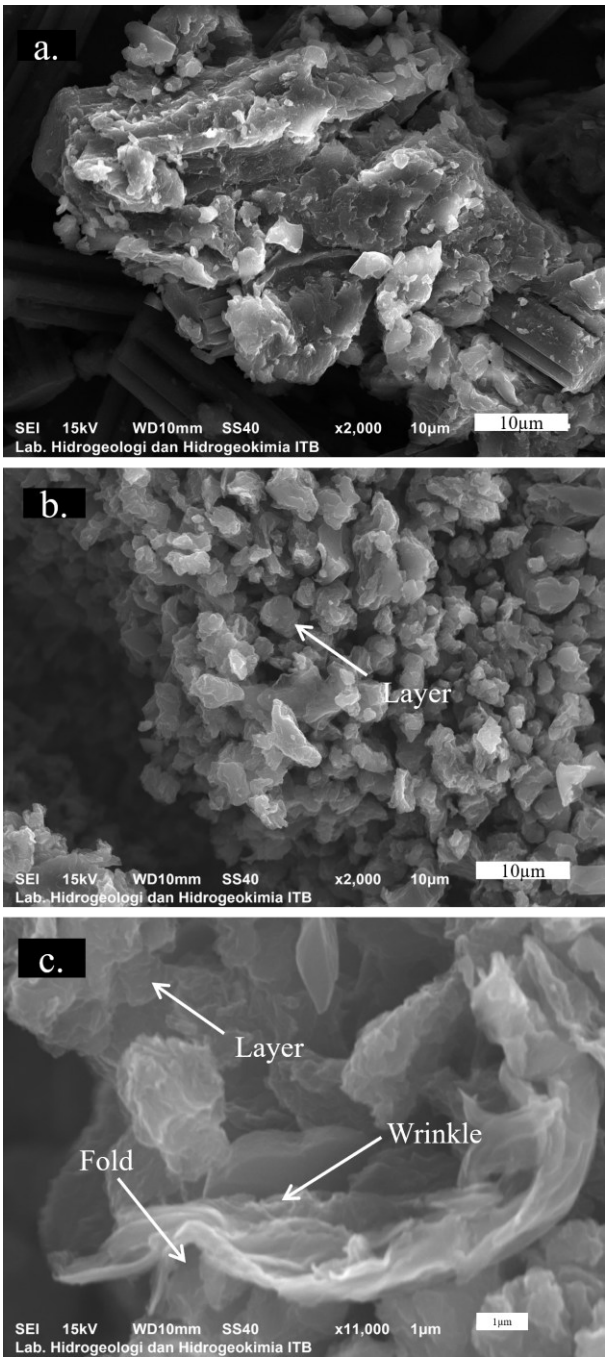

Figure 4. Surface morphology: a) GrO grains, b) rGO grains with multiple layers, and c) layers showing folds and wrinkles on rGO

SEM-EDX analysis was conducted on GrO and rGO to evaluate morphology, elemental composition, and the C/O ratio. rGO images (Figure 4b) at 2000× magnification show irregular particle shapes and sizes, while at 11,000× magnification (Figure 4c), wrinkles and folds are evident, likely resulting from thermal fluctuations during reduction at 180°C [27]. In comparison, the GrO image (Figure 4a) exhibits layered morphology, but the surface appears rougher than that of rGO.

In addition to the [002] peak shift from XRD analysis, EDX analysis was also carried out to determine the percentage of C and O atoms, which also confirms the success of the reduction process of GrO to rGO (Table 3). From the comparison value of the percentage of C and O atoms in GrO and rGO, it can be seen that there is a reduction in the number of O atoms after undergoing reduction, which indicates the success of the reduction process, with the C/O value increasing from 2.42 to 5.39.

Furthermore, Raman spectroscopy was also used to confirm rGO's multilayer structure. Raman spectroscopy is a key technique for analyzing graphene-based materials, as carbon allotropes exhibit characteristic peaks at approximately 1350, 1580, and 2700 cm^{-1} [28, 29, 30]. Figure 5a shows typical Raman spectra of GrO and rGO, where the D, G, and 2D peaks appear at 1347, 1597, and 2675 cm^{-1}, respectively, representing the main features of graphene-based materials.

The degree of graphitization was evaluated by deconvoluting the Raman spectra into four peaks: D_4 (also called D*, 1200 cm^{-1}), D1 (D, 1340 cm^{-1}), D_3 (D", 1500 cm^{-1}), and G (~1590 cm^{-1}). Peaks D_1 and D_4 correspond to disordered carbon with A_{1g} symmetry, D_3 represents amorphous carbon, and G indicates ideal graphitic carbon with sp^2 symmetry (E_{2g}) [31, 32, 33].

Figure 5b presents the deconvolution of the D and G peaks for GrO, with D_4 at 1200 cm^{-1}, D_1 at 1350 cm^{-1}, D_3 at 1500 cm^{-1}, and G at 1595 cm^{-1}. The I_{D1}/I_G ratio (D_1 peak area to G peak area) was used to assess structural defects, while the I_G/I_{D3} ratio indicated the degree of graphitization. The I_{2D}/I_G ratio (2D peak to G peak intensity) provides an estimate of the number of graphene layers [30, 31]. As shown in Table 4, GrO exhibited a defect level (I_{D1}/I_G) of 1.617 and a graphitization degree (I_G/I_{D3}) of 1.040.

Figure 5c shows the deconvoluted Raman spectrum of rGO, with D_4 at 1203 cm^{-1}, D_1 at 1348 cm^{-1}, D_3 at 1495 cm^{-1}, and G at 1595 cm^{-1}. The I_{D1}/I_G ratio for rGO was 1.771, consistent with the classification of graphene derivatives reported by King *et al.* [34], indicating a reduction in defects compared to GrO. The increased intensity of the G band and the decreased intensity of the 2D band suggest an increase in the number of graphene layers [30, 31].

Graphite oxide contains various oxygen functional groups, including epoxy, hydroxyl, and carbonyl, which disrupt the sp^2 network and convert some carbon atoms to sp^3 hybridization. This structural disruption is reflected in the rougher morphology of GrO observed in SEM images (Figure 4a). The hydrothermal reduction process removes a significant portion of these oxygen groups, partially restoring the conductive sp^2 network. However, the reduction is not complete, leaving residual defects such as vacancies, lattice distortions, and remaining oxygen groups. These residual defects are reflected in the I_{D1}/I_G value for rGO and corroborated by the wrinkles and folds observed in SEM images (Figure 4c).

The I_G/I_{D3} ratio is used to evaluate the degree of graphitization, reflecting the extent to which carbon atoms are arranged in a regular and dense hexagonal graphite structure [35]. The value obtained for rGO was 1.039, which is similar to that of GrO (1.040), indicating that the graphite crystal structure of GrO was largely retained in the synthesized rGO.

Table 3. GrO and rGO parameters from XRD and SEM-EDX

Sample	Graphite [25]	GrO	rGO
2θ (°) [002] peak	26.72	10.44	25.26
d_{002} (nm)	3.330	0.845	0.352
% C	-	67.62	83.63
% O	-	27.91	15.50
C/O	-	2.420	5.390

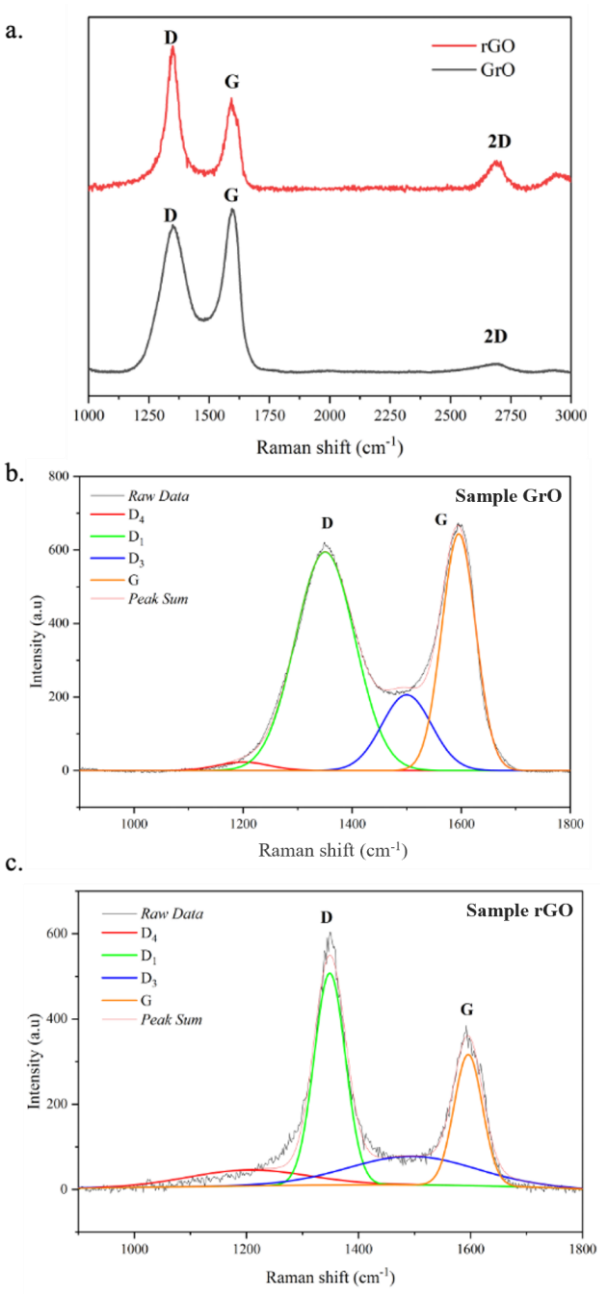

Figure 5. (a) Raman spectra of GrO and rGO (laser excitation wavelength 532 nm), (b) deconvolution of D and G bands for GrO, and (c) deconvolution of D and G bands for rGO

Table 4. Raman spectral features of GrO and rGO obtained from the deconvolution of the D and G bands

Parameter	GrO value	rGO value	Reference value	Reference
I_{D1}/I_G	1.617	1.771	1.12	[34]
I_G/I_{D3}	1.040	1.039	-	[35]
I_{2D}/I_G	0.055	0.321	<1	[36, 37]

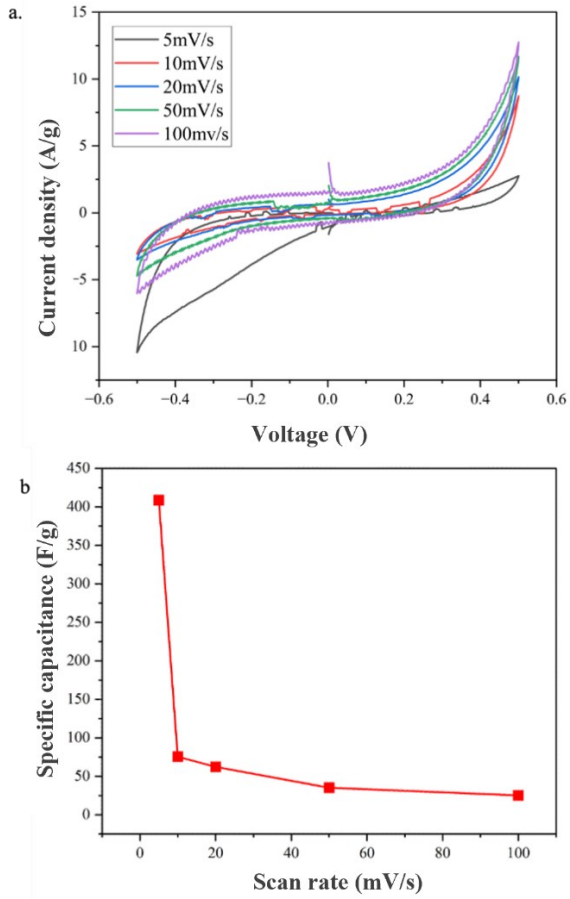

Figure 6. (a) CV curves of rGO at different scan rates and (b) specific capacitance of rGO as a function of scan rate

The 2D peak, observed around 2700 cm^{-1}, arises from a second-order Raman scattering process and is a characteristic feature of graphitic carbon materials, indicating the presence of graphene layers [32, 38]. The I_{2D}/I_G intensity ratio is used to estimate the number of graphene layers: values of ~2–3 correspond to monolayer graphene, $1 < I_{2D}/I_G < 2$ indicate bilayer graphene, and $I_{2D}/I_G < 1$ indicates multilayer graphene [36, 37]. In this study, the I_{2D}/I_G ratio for rGO was 0.321, confirming that the material consists of multilayer graphene. All calculated Raman parameters are summarized in Table 4.

Following material characterization, electrochemical analysis was performed to evaluate the suitability of rGO as a supercapacitor electrode. CV was employed to assess the electrochemical behavior of rGO, including its capacitance, stability, redox characteristics, and electron transfer mechanisms. CV measurements were conducted using a three-electrode system comprising a working electrode, a reference electrode, and a counter electrode [39].

Figure 6a presents the CV profiles of rGO at five different scan rates [40]. The curves exhibit a nearly rectangular shape, indicative of electric double-layer capacitance behavior and characteristic of supercapacitor materials. The specific capacitance of rGO was calculated from the CV data using Equation (4) [7, 41], as shown in Figure 6b.

$$Cs = \frac{\int I\,dV}{m.v.\Delta V} \quad (4)$$

Where, m is the mass of the active material (g), s is the scan rate (V/s), $\Delta V = |V_2 - V_1|$ is the potential window width, and I is the current response at a given potential V.

After calculating the specific capacitance at each scan rate, the results shown in Figure 6b indicate a decrease in capacitance with increasing scan rate. This behavior is attributed to the accelerated oxidation–reduction processes at higher scan rates, which limit the charge storage capability of the rGO electrode. The redox reactions on the electrode surface generate measurable currents at specific potentials. At the lowest scan rate (5 mV/s), the specific capacitance reached 408.661 F/g, with a large cathodic current allowing for maximum charge storage.

The pseudocapacitive behavior of rGO arises from faradaic reactions involving residual oxygen functional groups, such as hydroxyl and carbonyl groups, as well as structural defects that serve as active sites for redox interactions between the electrode and electrolyte ions. As the scan rate increases, the current response becomes less stable, and the oxidation-reduction processes accelerate, resulting in a notable decrease in capacitance, particularly between 5 mV/s and 10 mV/s. Higher scan rates lead to a decrease in specific capacitance due to limitations in ion transport at the electrode and other kinetic constraints [40]. This indicates that CV measurements are more representative when conducted at slower scan rates.

4. Conclusion

In this study, rGO was successfully synthesized through a combination of a modified Hummers method and a hydrothermal reduction process, resulting in high-quality structures. XRD analysis confirmed the transformation to rGO, showing interlayer distances of 0.35–0.40 nm, a crystalline and multilayer structure, with crystallite sizes of L_a = 5.825 nm and L_c = 0.967 nm. Raman spectroscopy revealed an increased structural irregularity, with I_{D1}/I_G = 1.771, I_G/I_{D3} = 1.039, indicating a high degree of graphitization, and I_{2D}/I_G = 0.321 confirming the multilayer nature of the material. Electrochemical analysis using cyclic voltammetry demonstrated that the performance of rGO is influenced by its degree of reduction and porous structure. The maximum specific capacitance of 408.661 F/g was observed at a scan rate of 5 mV/s, while higher scan rates (>10 mV/s) caused a significant decrease in capacitance due to kinetic limitations. These findings highlight the potential of the synthesized rGO for energy storage applications, such as supercapacitors or battery electrodes, and suggest that CV measurements at lower scan rates (<5 mV/s) are optimal for future studies.

Acknowledgment

This research was supported by the Directorate General of Higher Education, Research, and Technology, Ministry of Education, Culture, Research, and Technology, and LPPM UNPAR through the 2024 Regular Fundamental Research Grant (No. III/LPPM/2024-06/108-PE).

References

[1] Raluca Tarcan, Otto Todor-Boer, Ioan Petrovai, Cosmin Leordean, Simion Astilean, Ioan Botiz, Reduced graphene oxide today, *Journal of Materials Chemistry C*, 8, 4, (2020), 1198-1224 https://doi.org/10.1039/C9TC04916A

[2] A. K. Geim, Graphene: Status and Prospects, *Science*, 324, 5934, (2009), 1530-1534 https://doi.org/10.1126/science.1158877

[3] Songfeng Pei, Hui-Ming Cheng, The reduction of graphene oxide, *Carbon*, 50, 9, (2012), 3210-3228 https://doi.org/10.1016/j.carbon.2011.11.010

[4] Dilek Öztekin, Hüseyin Arbağ, Sena Yaşyerli, Preparation of RGO with Enhanced Electrical Conductivity: Effects of Sequential Reductions of L-Ascorbic Acid and Thermal, *Arabian Journal for Science and Engineering*, 50, 13, (2025), 9905-9918 https://doi.org/10.1007/s13369-024-09915-5

[5] Wei Liu, Giorgio Speranza, Tuning the Oxygen Content of Reduced Graphene Oxide and Effects on Its Properties, *ACS Omega*, 6, 9, (2021), 6195-6205 https://doi.org/10.1021/acsomega.0c05578

[6] Maria Iliut, Ana-Maria Gabudean, Cosmin Leordean, Timea Simon, Cristian-Mihail Teodorescu, Simion Astilean, Riboflavin enhanced fluorescence of highly reduced graphene oxide, *Chemical Physics Letters*, 586, (2013), 127-131 https://doi.org/10.1016/j.cplett.2013.09.032

[7] Yao Chen, Xiong Zhang, Dacheng Zhang, Peng Yu, Yanwei Ma, High performance supercapacitors based on reduced graphene oxide in aqueous and ionic liquid electrolytes, *Carbon*, 49, 2, (2011), 573-580 https://doi.org/10.1016/j.carbon.2010.09.060

[8] Prasad Eknath Lokhande, Umesh S. Chavan, Abhishek Pandey, Materials and Fabrication Methods for Electrochemical Supercapacitors: Overview, *Electrochemical Energy Reviews*, 3, 1, (2020), 155-186 https://doi.org/10.1007/s41918-019-00057-z

[9] M. Aulice Scibioh, B. Viswanathan, Chapter 3 - Electrode materials for supercapacitors, in: M.A. Scibioh, B. Viswanathan (Eds.) *Materials for Supercapacitor Applications*, Elsevier, 2020, https://doi.org/10.1016/B978-0-12-819858-2.00003-2

[10] Daniel R. Dreyer, Sungjin Park, Christopher W. Bielawski, Rodney S. Ruoff, The chemistry of graphene oxide, *Chemical Society Reviews*, 39, 1, (2010), 228-240 https://doi.org/10.1039/B917103G

[11] James E. Ellis, Dan C. Sorescu, Seth C. Burkert, David L. White, Alexander Star, Uncondensed Graphitic Carbon Nitride on Reduced Graphene Oxide for Oxygen Sensing via a Photoredox Mechanism, *ACS Applied Materials & Interfaces*, 9, 32, (2017), 27142-27151 https://doi.org/10.1021/acsami.7b06017

[12] Linh T. Le, Matthew H. Ervin, Hongwei Qiu, Brian E. Fuchs, Woo Y. Lee, Graphene supercapacitor electrodes fabricated by inkjet printing and thermal reduction of graphene oxide, *Electrochemistry Communications*, 13, 4, (2011), 355-358 https://doi.org/10.1016/j.elecom.2011.01.023

[13] Krzysztof Tadyszak, Jacek K. Wychowaniec, Jagoda Litowczenko, Biomedical Applications of Graphene-Based Structures, *Nanomaterials*, 8, 11, (2018), 944 https://doi.org/10.3390/nano8110944

[14] Dimitrios G. Trikkaliotis, Achilleas K. Christoforidis, Athanasios C. Mitropoulos, George Z. Kyzas, Graphene Oxide Synthesis, Properties and Characterization Techniques: A Comprehensive Review, *ChemEngineering*, 5, 3, (2021), 64 https://doi.org/10.3390/chemengineering5030064

[15] Rashad Al-Gaashani, Yahya Zakaria, One-Sun Lee, Janarthanan Ponraj, Viktor Kochkodan, Muataz A. Atieh, Effects of preparation temperature on production of graphene oxide by novel chemical processing, *Ceramics International*, 47, 7, Part A, (2021), 10113-10122 https://doi.org/10.1016/j.ceramint.2020.12.159

[16] William S. Hummers, Jr., Richard E. Offeman, Preparation of Graphitic Oxide, *Journal of the American Chemical Society*, 80, 6, (1958), 1339-1339 https://doi.org/10.1021/ja01539a017

[17] Adere Tarekegne Habte, Delele Worku Ayele, Synthesis and Characterization of Reduced Graphene Oxide (rGO) Started from Graphene Oxide (GO) Using the Tour Method with Different Parameters, *Advances in Materials Science and Engineering*, 2019, 1, (2019), 5058163 https://doi.org/10.1155/2019/5058163

[18] Daniela C. Marcano, Dmitry V. Kosynkin, Jacob M. Berlin, Alexander Sinitskii, Zhengzong Sun, Alexander Slesarev, Lawrence B. Alemany, Wei Lu, James M. Tour, Improved Synthesis of Graphene Oxide, *ACS Nano*, 4, 8, (2010), 4806-4814 https://doi.org/10.1021/nn1006368

[19] Allen J. Bard, Larry R. Faulkner, Electrochemical Methods: Fundamentals and Applications, *Russian Journal of Electrochemistry*, 38, 12, (2002), 1364-1365 https://doi.org/10.1023/A:1021637209564

[20] Agung Nugroho, Farhan Erviansyah, Dita Floresyona, Savisha Mahalingam, Abreeza Manap, Nurfanizan Afandi, K. Lau, C. Chia, Synthesis and characterization NS-reduced graphene oxide hydrogel and its electrochemical properties, *Letters on Materials*, 12, 2, (2022), 169-174 https://doi.org/10.22226/2410-3535-2022-2-169-174

[21] Marcos Alves Santos, Lucas Marques, Cecilia de Carvalho Castro Silva, Purification of graphene oxide dispersions by using a fluidic cell, *Analytical Methods*, 12, 28, (2020), 3575-3581 https://doi.org/10.1039/D0AY00600A

[22] L. Stobinski, B. Lesiak, A. Malolepszy, M. Mazurkiewicz, B. Mierzwa, J. Zemek, P. Jiricek, I. Bieloshapka, Graphene oxide and reduced graphene oxide studied by the XRD, TEM and electron spectroscopy methods, *Journal of Electron Spectroscopy and Related Phenomena*, 195, (2014), 145-154 https://doi.org/10.1016/j.elspec.2014.07.003

[23] N. S. Saenko, The X-ray diffraction study of three-dimensional disordered network of nanographites: Experiment and theory, *Physics Procedia*, 23, (2012), 102-105 https://doi.org/10.1016/j.phpro.2012.01.026

[24] Ning Sun, Zhaoruxin Guan, Yuwen Liu, Yuliang Cao, Qizhen Zhu, Huan Liu, Zhaoxiang Wang, Peng Zhang, Bin Xu, Extended "Adsorption–Insertion" Model: A New Insight into the Sodium Storage Mechanism of Hard Carbons, *Advanced Energy Materials*, 9, 32, (2019), 1901351 https://doi.org/10.1002/aenm.201901351

[25] Baitoul Mimouna, Mohammed Khenfouch, Malik Maaza, Ulrich Buttner, Synthesis and Characterization of Mass Produced High Quality Few Layered Graphene Sheets via a Chemical Method, *Graphene*, 3, (2014), 7-13 https://doi.org/10.4236/graphene.2014.32002

[26] Daniel Torres, Sara Pérez-Rodríguez, David Sebastián, José Luis Pinilla, María Jesús Lázaro, Isabel Suelves, Capacitance Enhancement of Hydrothermally Reduced Graphene Oxide Nanofibers, *Nanomaterials*, 10, 6, (2020), 1056 https://doi.org/10.3390/nano10061056

[27] A. Young Lee, Kihyuk Yang, Nguyen Duc Anh, Chulho Park, Seung Mi Lee, Tae Geol Lee, Mun Seok Jeong, Raman study of D* band in graphene oxide and its correlation with reduction, *Applied Surface Science*, 536, (2021), 147990 https://doi.org/10.1016/j.apsusc.2020.147990

[28] H. Cheun Lee, Wei-Wen Liu, Siang-Piao Chai, Abdul Rahman Mohamed, Azizan Aziz, Cheng-Seong Khe, N. M S. Hidayah, U. Hashim, Review of the synthesis, transfer, characterization and growth mechanisms of single and multilayer graphene, *RSC Advances*, 7, 26, (2017), 15644-15693 https://doi.org/10.1039/C7RA00392G

[29] Manonmani Mohandoss, Soujit Sen Gupta, Anith Nelleri, T. Pradeep, Shihabudheen M. Maliyekkal, Solar mediated reduction of graphene oxide, *RSC Advances*, 7, 2, (2017), 957-963 https://doi.org/10.1039/C6RA24696F

[30] Roksana Muzyka, Sabina Drewniak, Tadeusz Pustelny, Maciej Chrubasik, Grażyna Gryglewicz, Characterization of Graphite Oxide and Reduced Graphene Oxide Obtained from Different Graphite Precursors and Oxidized by Different Methods Using Raman Spectroscopy, *Materials*, 11, 7, (2018), 1050 https://doi.org/10.3390/ma11071050

[31] Ratna Frida Susanti, Stevanus Alvin, Jaehoon Kim, Toward high-performance hard carbon as an anode for sodium-ion batteries: Demineralization of biomass as a critical step, *Journal of Industrial and Engineering Chemistry*, 91, (2020), 317-329 https://doi.org/10.1016/j.jiec.2020.08.016

[32] Ying ying Wang, Zhen hua Ni, Ting Yu, Ze Xiang Shen, Hao min Wang, Yi hong Wu, Wei Chen, Andrew Thye Shen Wee, Raman Studies of Monolayer Graphene: The Substrate Effect, *The Journal of Physical Chemistry C*, 112, 29, (2008), 10637-10640 https://doi.org/10.1021/jp8008404

[33] Vittorio Scardaci, Giuseppe Compagnini, Raman Spectroscopy Investigation of Graphene Oxide Reduction by Laser Scribing, *C*, 7, 2, (2021), 48 https://doi.org/10.3390/c7020048

[34] Alice A. K. King, Benjamin R. Davies, Nikan Noorbehesht, Peter Newman, Tamara L. Church, Andrew T. Harris, Joselito M. Razal, Andrew I. Minett, A New Raman Metric for the Characterisation of Graphene oxide and its Derivatives, *Scientific Reports*, 6, 1, (2016), 19491 https://doi.org/10.1038/srep19491

[35] Xiang Xu, Daiyong Cao, Yingchun Wei, Anmin Wang, Gaojian Chen, Tianyuan Wang, Guixiang Wang, Xinli Chen, Impact of Graphitization Degree on the Electrochemical and Thermal Properties of Coal, *ACS Omega*, 9, 2, (2024), 2443-2456 https://doi.org/10.1021/acsomega.3c06871

[36] Van Tu Nguyen, Huu Doan Le, Van Chuc Nguyen, Thi Thanh Tam Ngo, Dinh Quang Le, Xuan Nghia Nguyen, Ngoc Minh Phan, Synthesis of multi-layer graphene films on copper tape by atmospheric pressure chemical vapor deposition method, *Advances in Natural Sciences: Nanoscience and Nanotechnology*, 4, 3, (2013), 035012 https://doi.org/10.1088/2043-6262/4/3/035012

[37] Alfonso Reina, Xiaoting Jia, John Ho, Daniel Nezich, Hyungbin Son, Vladimir Bulovic, Mildred S. Dresselhaus, Jing Kong, Large Area, Few-Layer Graphene Films on Arbitrary Substrates by Chemical Vapor Deposition, *Nano Letters*, 9, 1, (2009), 30-35 https://doi.org/10.1021/nl801827v

[38] Li Sun, Chungui Tian, Yu Fu, Ying Yang, Jie Yin, Lei Wang, Honggang Fu, Nitrogen-Doped Porous Graphitic Carbon as an Excellent Electrode Material for Advanced Supercapacitors, *Chemistry – A European Journal*, 20, 2, (2014), 564-574 https://doi.org/10.1002/chem.201303345

[39] Noémie Elgrishi, Kelley J. Rountree, Brian D. McCarthy, Eric S. Rountree, Thomas T. Eisenhart, Jillian L. Dempsey, A Practical Beginner's Guide to Cyclic Voltammetry, *Journal of Chemical Education*, 95, 2, (2018), 197-206 https://doi.org/10.1021/acs.jchemed.7b00361

[40] Agung Nugroho, Muhammad Reza Wirayudha Pratama, Hans Kristianto, Haryo Satriya Oktaviano, Arenst Andreas Arie, Ratna Frida Susanti, Synthesis and Electrochemical Properties of SnO_2 Composited Activated Carbon from Coffee Ground Waste for Supercapacitor Applications, *Jurnal Kimia Sains dan Aplikasi*, 26, 8, (2023), 293-299 https://doi.org/10.14710/jksa.26.8.293-299

[41] Xiang Ying Chen, Chong Chen, Zhong Jie Zhang, Dong Hua Xie, Gelatin-derived nitrogen-doped porous carbon *via* a dual-template carbonization method for high performance supercapacitors, *Journal of Materials Chemistry A*, 1, 36, (2013), 10903-10911 https://doi.org/10.1039/C3TA12328F